Surface & Coatings Technology 205 (2011) 3043–3049

Contents lists available at ScienceDirect

Surface & Coatings Technology

journal homepage: www.elsevier.com/locate/surfcoat

Corrosion behaviour of medical CoCr alloy after nitrogen plasma immersion ion implantation

J. Lutz [a,b,*], C. Díaz [c], J.A. García [c], C. Blawert [d], S. Mändl [b]

[a] Translational Centre for Regenerative Medicine, 04103 Leipzig, Germany
[b] Leibniz-Institut für Oberflächenmodifizierung, 04318 Leipzig, Germany
[c] AIN Centro de Ingeniería Avanzada de Superficies, 31191 Cordovilla - Pamplona, Spain
[d] Institut für Werkstoffforschung, GKSS Forschungszentrum Geesthacht, 21502 Geesthacht, Germany

ARTICLE INFO

Article history:
Received 12 August 2010
Accepted in revised form 5 November 2010
Available online 11 November 2010

Keywords:
CoCr
Corrosion
Biocompatibility
PIII

ABSTRACT

Surface treatment of medical CoCr alloys L605 by nitrogen plasma immersion ion implantation (PIII) leads to the formation of a hard and wear resistant surface layer, consisting of nitrogen in solid solution. However, a detailed investigation of the corrosion properties by potentiodynamic polarization and electrochemical impedance spectroscopy shows that even at processing temperatures of 350 °C, where no CrN precipitates are observed, no complete passivation of the surface by formation of a protective Cr_2O_3 layer is possible leading to enhanced corrosion rates further increasing with increasing PIII processing temperature. It is postulated that the enhanced affinity of chromium for nitrogen leads to a reduced mobility inside the alloy, thus prohibiting a timely surface passivation. Nevertheless, a surface modification where a moderate decrease in corrosion resistance coupled with a significant reduction in generated wear particles should be feasible for biomedical applications.

1. Introduction

Advances in metallic biomaterials have improved considerably the quality of life and life expectancy over the last fifty years, with applications ranging from endoprostheses, fracture fixation devices to intravascular implants [1]. Besides a beneficial combination of mechanical strength and ductility, high yield strength, low to moderate elastic modulus, excellent corrosion properties are required for these materials, with titanium alloys, CoCr, austenitic stainless and NiTi commonly used [2,3]. However, a persistent low release rate of metallic cations as well as wear particles is still present in these systems. Accordingly, a large amount of literature exists detailing the interaction of these by-products with human and animal tissue, as well as several surface treatment methods to assuage these problems.

Wear particles itself in the immediate vicinity of protheses stimulate macrophages and lymphocytes to produce proinflammatory mediators, which in turn enhance osteoclast formation, thus inducing osteolysis [4–6]. In addition, macrophages can transform towards osteoclast-like cells capable of resorbing bone after having phagocytosed wear particles [7]. Furthermore, spreading of wear particles through the whole body and accumulation in organs, as spleen, liver and lung with concurrent negative effects have been observed [8–10]. These processes are observed for different kinds of wear particles, indicating only a minor influence of the chemistry for nanoparticles [11–13].

In contrast, metallic cations act highly specific when inducing a tissue response. Ni ions induce cell death in endothelial cells by necrosis [14]. However, the release rate depends strongly on the materials chemistry with NiTi itself showing rather low release rates compared to stainless steel or CoCr alloys [15]. For Co^{2+} ions, multiple pathways have been identified depending on the local concentration, including apoptosis, increased expression of HIF-1α for endothelial cells [16] and increased osteoclasts activity [17].

Nevertheless, CoCr alloys are routinely employed in biomedical applications as they combine outstanding yield strength with a moderate elastic modulus of about 200 MPa and rather low wear rates [18]. The formation of a passive surface film on these alloys, consisting of an oxide highly enriched in Cr, with additions of Mo having a further beneficial effect, is responsible for this behaviour [19,20]. Nevertheless, generation of nanoparticles by mechanical wear processes is still observed in some total hip replacements (THRs) after explantation [21]. Besides, fretting corrosion may lead to the release of toxic ions such as Co, Cr and Ni, with Co predominantly found in the serum [22,23].

The number of publications reporting on surface modification of CoCr alloys by energetic ions is rather limited. Some information on plasma surface alloying [24], conventional beamline nitrogen ion implantation [25] or high intensity plasma ion nitriding [26,27] is available. All these experiments, including previous experiments on nitriding by plasma immersion ion implantation (PIII) [28,29],

* Corresponding author. Leibniz-Institut für Oberflächenmodifizierung, Permoserstr. 15, 04318 Leipzig, Germany. Tel.: +49 341 235 2944; fax: +49 341 235 2313.
E-mail address: jlutz@trm.uni-leipzig.de (J. Lutz).

0257-8972/$ – see front matter © 2010 Elsevier B.V. All rights reserved.
doi:10.1016/j.surfcoat.2010.11.017

typically show an increase of the surface hardness to 15–20 GPa in combination with a wear rate reduced by a factor of 10–100. These improved mechanical properties are caused by the insertion of up to 35 at.% nitrogen in the near surface region, extending up to 10 μm below the surface. Below 400–450 °C, a supersaturated expanded austenitic structure with nitrogen on interstitial sites is present while the precipitation of CrN and Cr_2N is observed at higher temperatures, together with a remaining austenitic CoNi-rich phase [24,30].

However, a selective increase in the cobalt ion release rate, while no significant change in nickel or chromium release was obtained even for samples showing nitrogen in solid solution [31]. In contrast, a threshold for the onset of an increased corrosion current corresponding to the formation of CrN precipitates is observed for nitrogen implantation into austenitic stainless steel [32]. However, no detailed investigation of corrosion properties itself has been published until now. In this study, results on electrochemical investigations of medical CoCr alloy with and without surface modification are presented.

2. Materials and methods

The wrought alloy L605 (20 wt.% Cr, 10 wt.% Ni, 15 wt.% W, 3 wt.% Fe, 1.5 wt.% Mn, balance Co; according to ASTM F-90) is a nonmagnetic alloy possessing good oxidation and corrosion resistance generally used for cardiovascular stents or artificial heart valves [33]. Flat disks were cut from a rod with a diameter of 20 mm, ground and polished to a mirror like finish. The typical grain size of the austenitic face centred cubic (fcc) structure was between 50 and 200 μm with all alloying elements in solid solution, except small WC precipitates.

Nitrogen insertion by PIII was performed in an ultra-high vacuum chamber at a base pressure of 10^{-6} Pa. At a nitrogen gas flow rate of 150 sccm, the resulting pressure during the experiments was 0.53 Pa. The plasma was generated by an electron cyclotron resonance plasma source operating at a power of 150 W and frequency of 2.45 GHz. The resulting electron temperature and plasma density in front of the substrate holder were 1.3 eV and 1.6×10^{10} cm^{-3}, respectively, as determined from Langmuir probe measurements. Negative high voltage pulses of 10 kV with a rise time of 10 ns/kV and total length of 15 μs were applied to the substrate holder. The process temperature was between 350 and 550 °C, as determined with a pyrometer calibrated against a thermocouple [34], for a total process time of 120 min [29]. The incident fluences were between 2.3×10^{18} and 8.0×10^{18} nitrogen ions/cm^2 which correspond to retained nitrogen fluences between 2.7×10^{18} and 6.8×10^{18} nitrogen ions/cm^2 as several desorption and adsorption processes take place during the pulse pauses [35]. Additionally, one set of samples implanted at 450 °C was subsequently implanted with oxygen in a second experiment at 450 °C for 60 min to study the influence of an artificial surface oxide layer – the question to be answered is whether this oxide on top of a modified CoCr alloy is more or less protective than the native oxide layer on an unmodified CoCr alloys – on the electrochemical properties. In the following, these samples are indicated with "thermal oxide".

The phase composition was studied by X-ray diffraction (XRD) in Bragg-Brentano geometry using Cu $K_{\alpha1}$ radiation. Quantitative depth-profiles of different elements were measured by glow discharge optical emission spectroscopy (GDOES) using a JY GD Profiler HR (Jobin-Yvon Horiba, France) RF source operating at 650 Pa and 40 W discharge [36]. Furthermore, scanning electron microscopy (SEM) was used to acquire qualitative images of the surfaces after ion bombardment and corrosion experiments.

Corrosion tests were performed on both the untreated and PIII treated alloy in the as received condition. All specimens were cleaned in ethanol prior to corrosion test. Electrochemical experiments were performed in Ringer solution (pH 6.2), saturated with atmospheric oxygen. The corrosion cell (333 ml) with a three electrode set-up consisted of an Ag/AgCl reference, a Pt counter electrode and the specimen as working electrode. The electrolyte temperature was controlled at 37.2 ± 0.2 °C and the electrolyte was stirred during the experiments. One experiment lasted up to 7 days and consisted of three subsequent tests as listed below.

1. 120 minute recording of the free corrosion potential.
2. Potentiodynamic polarization scan starting from −200 mV relative to the free corrosion potential with a scan rate of 0.2 mV/s. The test was terminated when a corrosion current of 0.1 mA was exceeded to minimize the damage on the specimen surface before the next sequence started. From the cathodic branch of the polarization curve the corrosion rate was determined using the Tafel slope.
3. Electrochemical impedance spectroscopy (EIS) measurements at free corrosion potential were carried out using a Gill AC over the frequency range from 10 kHz to 0.01 Hz. The amplitude of the sinusoidal signals was 10 mV. The measurements were repeated at certain fixed times after the end of the previous sequence (2, 8 and 20 h for group A and 0, 2, 6, 12, 24, 48 and every 24 h until 168 h for group B). The charge transfer resistance was estimated assuming a simple Randles circuit model.

Samples investigated in the order (1-2-3) are labelled as group A. For the second half of the specimens the order of potentiodynamic polarisation and EIS measurements was changed, thus starting with EIS directly after the free corrosion potential measurement (1-3-2, labelled as group B). Thus, any influence of the potentiodynamic measurements or the electrochemical impedance spectroscopy on the surface properties itself should be detectable.

3. Results

For the samples implanted at 350 and 400 °C, an expanded austenitic lattice was found in the surface region with a total layer thickness of 1.2 and 1.8 μm. In contrast, the samples implanted at 450 and 550 °C developed CrN/Cr_2N precipitates while thicker layers of 4 and 4.5 μm were observed, respectively [29]. Typical elemental depth profiles obtained directly after nitrogen PIII are shown in Fig. 1, where a plateau-like nitrogen distribution extending from the surface down to 1.2 μm, followed by a rapid decay towards zero is observed. Within this nitride containing layer, a significant increase of the Cr/Co ratio by about 25% and a slight decrease of the Ni/Co ratio by 5% is observed, indicating Cr enrichment and a slight removal of Ni from this layer. However, these shifts in the ratios are already present in the as-polished samples. After oxygen implantation, an additional oxide layer of about 20 nm was observed on the surface. For the growth of the nitride layer, a thermal activation energy of about 0.8 eV was observed, in agreement with previously published results [30].

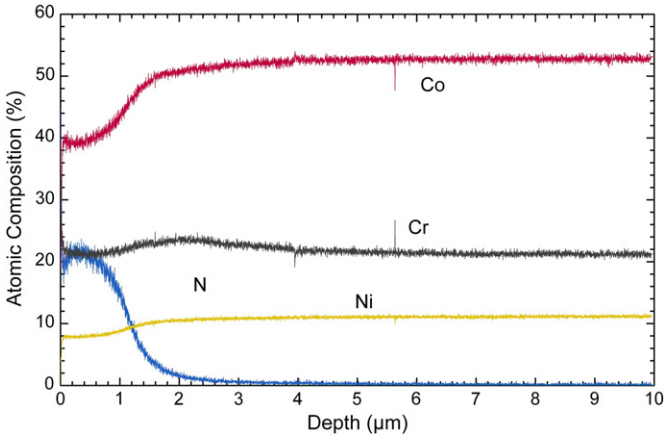

Fig. 1. Elemental depth profiles from GDOES measurements after nitrogen PIII at 350 °C.

In Fig. 2, the time evolution of the free corrosion potential is shown for the samples from group B. Nitrogen implantation at temperatures up to 400 °C does lead to a shift of the potential to more noble values, compared to the untreated control sample. These results suggest that the PIII treatment at lower temperatures establishes a passive film on the surface similar to what is produced by long term exposure to the Ringer solution and/or anodic polarization. However, the higher treatment temperature of 450 °C does have a negative effect on the ability to form passive films, despite the formation of a thermal oxide before the corrosion potential measurement. Here, the potential remains at lower values. One interesting feature is the initial quite negative free corrosion potential of the untreated samples, which requires exposure to Ringer solution of more than one day before a relatively stable corrosion potential is observed.

When analysing the polarisation curves, depicted in Fig. 3 for group A, similar tendencies are observed. The samples for the two low temperature treatments remain passive in the solution and the potentials are shifted by about 450 mV towards more positive values, compared to the untreated specimen. Although the corrosion resistance determined by Tafel slope evaluation is slightly reduced and the passive region is smaller compared to the untreated alloy the passive current density is lower. Nevertheless, similar breakthrough potentials are observed for the untreated sample and the two samples implanted with nitrogen at lower temperatures. In contrast, implantation at higher temperature, even with subsequent oxygen implantation, prevents the formation of a stable passive film. The active dissolution occurred straight after passing the corrosion potential. The corresponding corrosion rates determined from the Tafel slope, presented in Fig. 4, agree with this assessment. With increasing temperature during the PIII process, a monotonous increase of the corrosion rate, compared to the untreated specimen is observed without any trace of saturation of threshold behaviour.

After the polarisation measurements, EIS measurements were performed for group A samples. The obtained results confirm the measured corrosion rates. As can be seen in Fig. 5, the charge transfer resistance values estimated from fitting with a Randle circuit agree very well with the corrosion rates.

When starting first with the EIS measurements, group B, similar tendencies are observed. The corresponding Nyquist plots are shown in Fig. 6. The EIS results confirm that the corrosion resistance is decreasing with increasing treatment temperature. Best performance is found for the untreated material. However all materials reveal an increasing resistance with immersion time in Ringer solution indicating that some protective films form on the surfaces. The stability of those films is also decreasing with treatment temperature. The increase in corrosion resistance is much better for the untreated material in comparison to any of the treated materials, as can be seen from the changes in the charge transfer resistance depicted in Fig. 7.

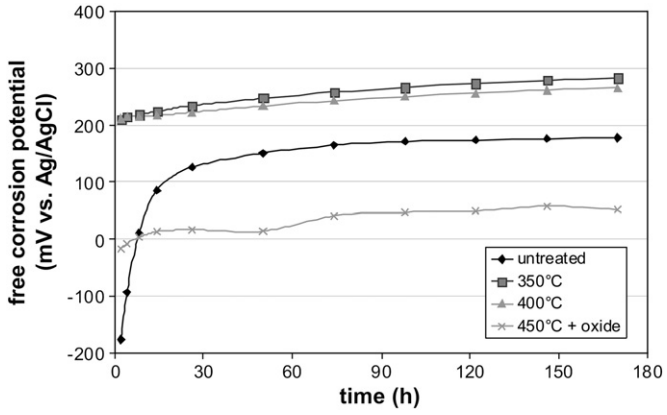

Fig. 2. Time evolution of the free corrosion potential for different samples (group B) in Ringer solution at 37.2 °C.

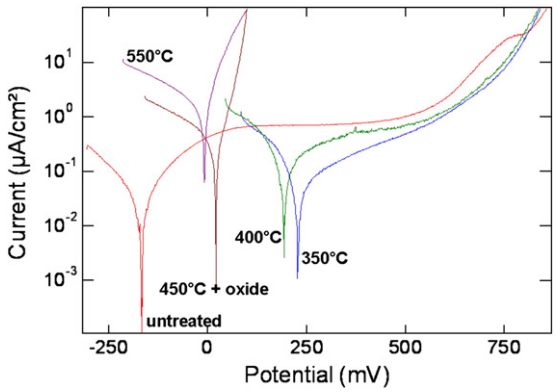

Fig. 3. Polarisation curves for different samples (group A) in Ringer solution at 37.2 °C.

Finally, the findings from polarisation experiments after EIS are plotted in Fig. 8. The results confirm that passive films are present on all specimens after 7 day immersion in Ringer solution. However the order of stability of those films is consistent with the charge transfer resistance values obtained from EIS confirming the detrimental influence of higher treatment temperatures. The lowest corrosion current is obtained for the untreated sample, followed by the samples at 350 and 400 °C and, with even higher values, the sample implanted with nitrogen at 450 °C, followed by thermal oxidation.

A representative elemental depth distribution after corrosion testing is presented in Fig. 9 for a sample previously implanted at 550 °C with nitrogen. The thickness of the nitrogen containing layer is strongly reduced, compared to the initial condition of 4.1 µm before corrosion testing. At the same time, a strong, selective reduction of the Co content is observed within the nitrogen rich zone, while the other elements do not show significant changes. Thus, owing to the diminished Co fraction, an increase of the concentration for the other elements is found near the surface, leading, e.g. to nitrogen concentration of 45% and more. In the immediate vicinity of the surface, an oxide layer is observed. As chromium nitride precipitates exist for this sample implanted at the very high temperature, a selective depletion of the Co-rich matrix leaves the precipitates intact without any noticeable nitrogen loss.

The remaining nitrogen is compared in Fig. 10 for both groups A&B. As can be seen, no difference between the two groups is presented, indicating that the order of the EIS and the potentiodynamic polarization measurements does not influence the final state of the samples. With increasing PIII treatment temperature, an enhancement of the absolute nitrogen concentration is observed, together with an augmented loss of the layer. For 550 °C, the remaining layer is even thinner than at 450 °C, while for 350 and 400 °C nearly identical thicknesses are observed in the final condition. No broadening of the

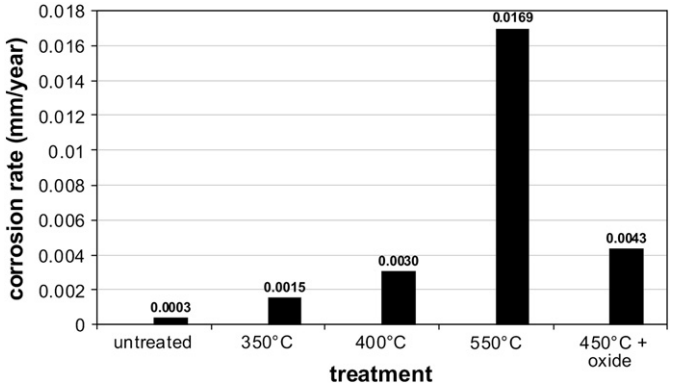

Fig. 4. Corrosion rates calculated from the polarisation curves shown in Fig. 2 as function of PIII temperature (group A).

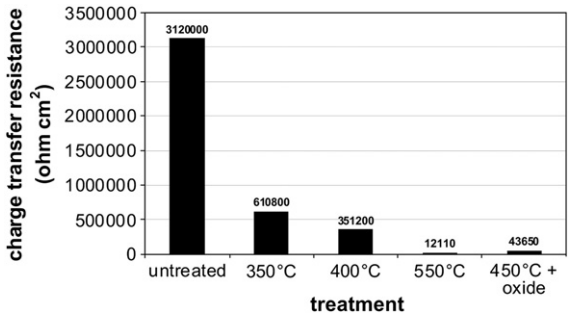

Fig. 5. Charge transfer resistance measured 2 h after the end of the polarisation measurement as function of PIII temperature (group A).

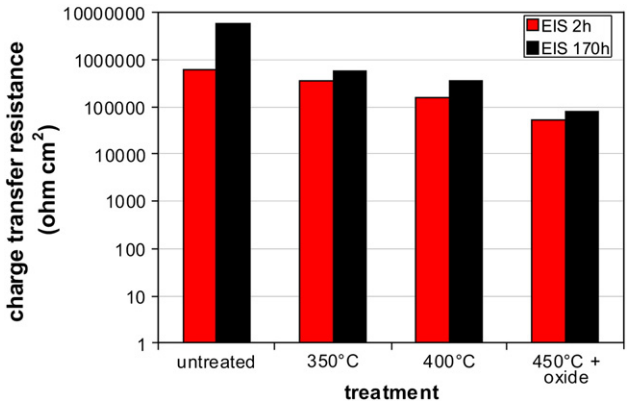

Fig. 7. Initial (2 h) and final (168 h) charge transfer resistance calculated from the Nyquist plots shown in Fig. 6 (assuming a simple Randle circuit) as function of PIII temperature (group B).

nitrogen profile is observed during corrosion testing for any of the samples, indicating no nitrogen mobility.

Detailing the relative amounts of the metallic constituents, the Cr/Co ratio is plotted in Fig. 11 as a function of depth. For all samples except for PIII at 550 °C, a strong, abrupt increase in the first 20–30 nm indicates the chromium rich surface oxide. For the sample with a thermal oxide formed after PIII, this layer is slightly thicker than for the other samples. A conspicuous Co depletion is observed within nitrided layer, together with a still noticeable depletion below the nitrided layer. Again, this effect scales with the PIII implantation temperature. For other metallic elements except cobalt, no variation was found, except for minor changes in the composition of the very thin surface oxide.

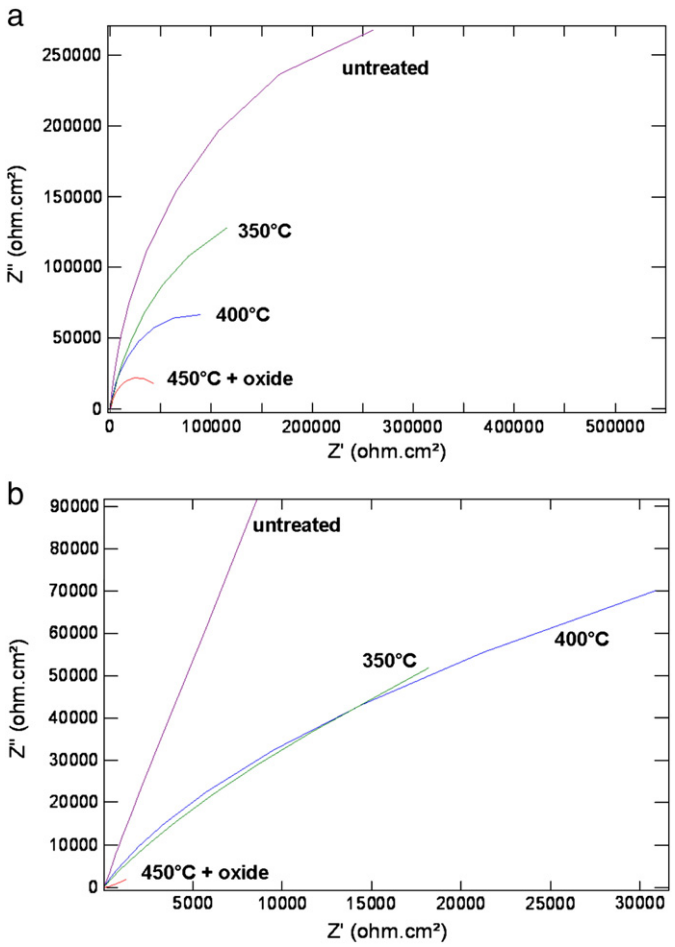

Fig. 6. Nyquist plots for different samples after immersion in Ringer solution at 37.2 °C (group B) for a) 2 h and b) 170 h, respectively.

4. Discussion

4.1. Passivation and corrosion processes

The corrosion results indicate that the most important element determine the electrochemical behaviour of the L605 alloy is chromium and its ability to form a passive Cr_2O_3 film. Considering that the pH value of the Ringer solution is about 6.2 the observed loss of passivity at about 600 mV visible in the polarisation scans shown in Fig. 2 is consistent with the loss of Cr_2O_3 due to CrO_4^{2-} formation. As a consequence the stable protecting oxide film is dissolving with further increasing potential and the current is strongly increasing. Considering the development of the free corrosion potential with time the native growth of the passive oxide film is rather slow in Ringer solution for the untreated alloy.

Nevertheless, this behaviour of a prolonged passivating reaction extending over several hours has already been reported in literature for CoCr alloys [37], leading to a passivating Cr_2O_3 rich surface layer for low (20 wt.% — as used in this investigation) and high Cr (28 wt.% — Co28Cr6Mo) contents, with additional molybdenum enhancing this effect [3,19]. However the wrought alloys according to ASTM F-90 with a lower Cr content are showing a slightly better corrosion behaviour than as-cast alloys according to ASTM F-75 [18]. As long as a bulk Cr concentration beyond 8–10 wt.% is present, the formation of a passivating network at the surface is present, allowing for a thermodynamically driven surface segregation [38].

Low temperature nitriding by PIII already generates a film similar to the passive oxide for untreated CoCr. Further studies are required to actually characterise the top layer on the PIII specimens, e.g. using XPS. After the PIII treatment when the samples are brought from

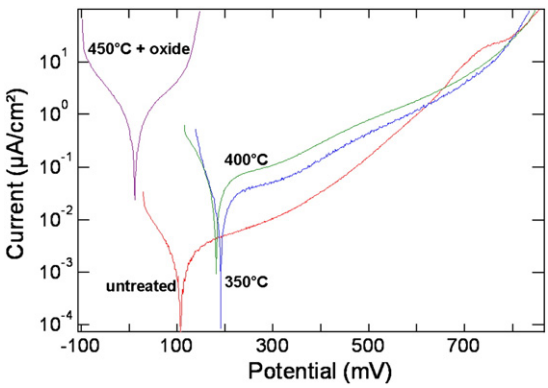

Fig. 8. Polarisation curves for different samples after 7 days immersion in Ringer solution (group B).

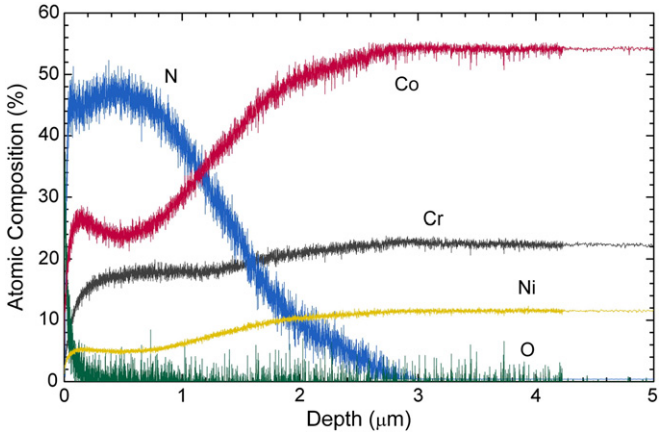

Fig. 9. Elemental depth profiles after corrosion testing: 550 °C, group A (please note that C, Fe and W were omitted for clarity, the sum of the presented five elements does not add up to 100%).

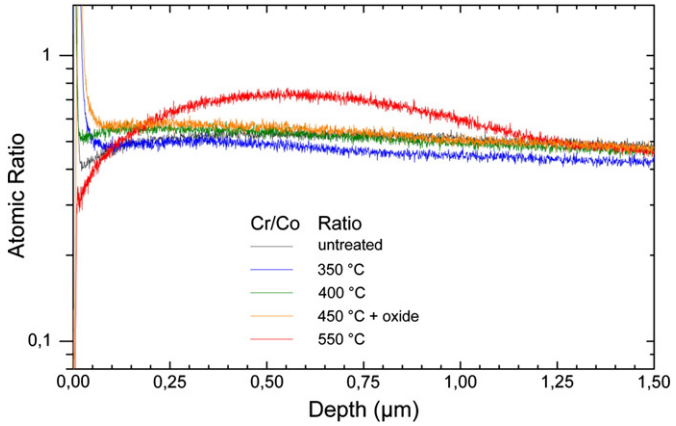

Fig. 11. Cr/Co and Ni/Co ratios as a function of depth after corrosion testing (group A). The only sample with a higher ratio at 0.5–1.0 μm is the sample implanted at 550 °C. Please note the logarithmic intensity scale.

vacuum to the atmosphere – normally at temperatures around 50–100 °C – a reaction of the surface with oxygen is occurring, thus a chromium oxide layer is forming on the outermost skin of the surface. This stable oxide film shifts the corrosion potential of the alloy to above 100 mV and obviously with growing thickness the potential is further increasing and can reach values close to 300 mV for longer immersion times (7 days). The low temperature PIII specimens (350 and 400 °C) have already starting values of around 200 mV due to the artificially formed oxide film during PIII. This implies that the short term protection as indicated by the passive current of the treated specimens is better compared with the untreated material. However in the long term the situations changes and the passive film forming on the untreated alloy is more protecting (cf. Figs. 3 and 8).

On the other hand, all other measurements already indicate the negative influence of the treatment temperature. The corrosion resistance is always decreasing with increasing temperature. However at low temperatures the decrease is still acceptable and passivity of the alloy is still available. When the temperature is increasing above 400 °C the formation of CrN is difficult to prevent. Unfortunately the passive film formation requires mobility of chromium to build the protecting Cr_2O_3 film at the surface. If chromium is bound in CrN there is not enough free chromium available to form the oxide film. Even without the formation of nitrides the presence of nitrogen in the lattice may affect the diffusivity of chromium.

It is known that nitrogen in expanded austenitic stainless steel is trapped by chromium [39]. This special interaction of nitrogen and chromium can slow down the diffusivity and therefore the ability of forming the passive film compared with the untreated material. This is consistent with the observed slight decrease of the corrosion resistance of treated specimens compared with the untreated alloy. With decreasing protectiveness of the chromium based passive film the dissolution of the other less noble alloying elements is increasing. In this case the dissolution of Co should be increasing, which is consistent with the experimental observations.

The direct transfer of the Cr trapping model for nitriding of austenitic stainless steel to CoCr alloys is supposed to be legitimate as very similar diffusion and phase formation behaviours are observed [29]. However, a certain hesitation is advised, as a direct correlation between either the nitrogen surface concentration or the threshold necessary for fast diffusion is not present, with the nitrogen content in the expanded austenitic structure for both stainless steel and CoCr alloys only weakly depending on the Cr content [40]. Furthermore, the N/Cr ratio is around 2.5 and 1.5 near the surface and at the transition from fast to slow diffusion, respectively. At the same time, a correlation with the solubility limit of the interstitial sublattice as the determining factor for at least the nitrogen content, in contrast to the diffusivity, is proposed [41]. XPS investigations are in progress for a detailed understanding of these processes, albeit beyond the scope of this presentation.

Finally it can be stated that despite these differences, the artificially chromium oxide films after different nitriding conditions are similar from an electrochemical point of view. The electrochemical potential is obviously determined by the thickness and/or stability of the layer independent whether it is formed slowly in the Ringer solution or fast during the anodic polarisation of the specimens during the potentiodynamic polarisation test or during the nitrogen PIII treatment. The only requirement for this behaviour is the presence of chromium which has still sufficient mobility in the lattice to form the oxide film. Latter is the case for the untreated material and the expanded austenite phase, but not if CrN has formed. Therefore a plasma oxidation treatment after a high temperature PIII treatment has almost no positive effect on the formation of a protective chromium oxide film anymore because most chromium is already tightly bonded to nitrogen.

The main difference between austenitic stainless steel and CoCr alloys, which are corrosion resistant in the native state, appear to be the different time constants for passivation, respective repassivation. Reduced mobilities encountered in surfaces nitrided at moderate temperatures of 350–400 °C do not lead to a compromised corrosion resistance for austenitic stainless steel, in contrast to CoCr alloys where the already slower mobility of Cr is reduced even further, leading to a compromised corrosion resistance. At higher temperatures, when CrN precipitates are formed thus completely immobilizing the chromium, corrosion processes are again observed for both materials.

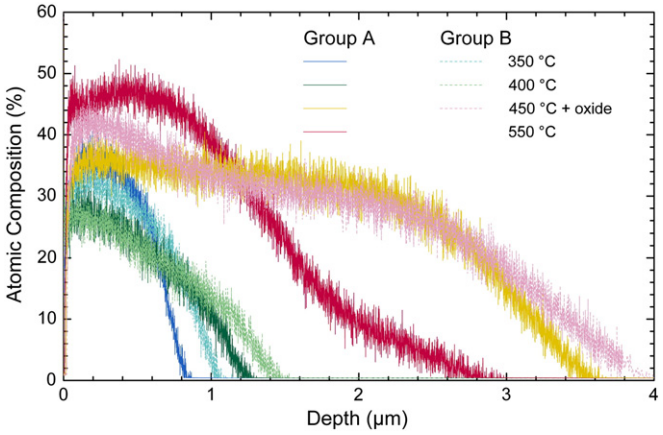

Fig. 10. Nitrogen depth profiles after corrosion testing (groups A and B).

4.2. Release of ions and implications for biomaterials

The surface morphology does not show significant differences before and after the corrosion experiments at different PIII treatment parameters. The roughness itself – which increases considerably during the PIII process to values of up to 250–300 nm R_a depending on the process temperature [42] – measured by an optical 3D profilometer with a lateral resolution of 0.3 μm and a vertical resolution better than 10 nm – does not change significantly during the corrosion test.

A detailed inspection of the surface by SEM, as presented in Fig. 12, shows a heavily corroded surface after 24 h for the 550 °C PIII treatment, together with a surface characterised by the decomposition into a Cr-poor matrix and CrN precipitates, and accompanied by dark areas consisting primarily of Cr_2O_3, as determined by EDX. In contrast, less severe damage is observable for the sample implanted at 350 °C where the basic fcc lattice with grain boundaries and dislocation faults is dominating, with enhanced contrast due to orientation dependent sputter yields. The bright spots are WC inclusions which do not present preferred sites for corrosive attack. No localized pitting corrosion is observed in either case, congruent with dissolution of the solid solution present at lower PIII temperature and the dissolution of the precipitate encountered at higher PIII temperatures.

The reduction of the layer thickness during the corrosion processes, increasing with increasing PIII process temperature is congruent with this viewpoint. However, own investigations [31] as well as literature results [25] indicate a selective increase of the Co ion release while Cr and Ni remain at a nearly constant, low level. Thus, an agreement with the predominant – although sometimes incomplete – formation of a protective Cr_2O_3 layer is found. Cobalt is released as Co(II) ions, remaining in solution, while Cr(III) form an insoluble oxide phase. The existence of soluble, toxic Cr(VI) found during transpassive dissolution of CoCr [20] can be negated for the present experiments. For nickel, the formation of NiO or $Ni(OH)_2$, both with very low solubilities, [43] is expected for the encountered pH value.

Additionally, a selective cobalt derichment of the surface layer is occurring, as can be seen from Fig. 11. It has to be pointed out that only a snapshot at the end of the corrosion tests is provided. The initial surface oxide is always to the left of the final surface shown here, thus a continuous cobalt loss with a partial chromium retention is observed during the corrosion tests. Thus, the predominant release of cobalt ions is partially related with a selective release and partially related with the solubilities of the corrosion products.

For biomedical applications, the PIII treatments presented here lead to a significant reduced wear rate and correspondingly lower particle generation [31], while the corrosion rate and ion release is increased with the absolute changes themselves depending on the process temperature for PIII nitriding. At lower processing temperatures of 350 °C and below, an increase in the corrosion rate by a factor of up to 5 is observed. Thus, for these conditions, the reduction in wear dominates over the increase in corrosion. In contrast, for higher processing temperatures the opposite effect is observed. When estimating the effectiveness of such a surface treatment, the relative toxicities of particles and ions have to be considered. For cobalt, nanoparticles are found to be much more toxic for mouse fibroblasts and human peripheral leukocytes than Co^{2+} ions [44,45]. Hence, changing the relative release rates towards more ions and less particles should be beneficial up to a certain degree.

5. Summary and conclusions

Using PIII, it is possible to form hard and wear resistant surface layers on CoCr alloys. However, even for very low processing temperatures, the corrosion resistance is always less pronounced than for untreated base material. Ostensibly, the transient formation of Cr–N bonds at low temperatures, leading to the formation of an expanded austenitic lattice, reduces the Cr mobility enough to fall below a threshold necessary to sustain the continuing formation of a passivating surface oxide, already occurring much slower than for austenitic stainless steels with a comparable chromium content and

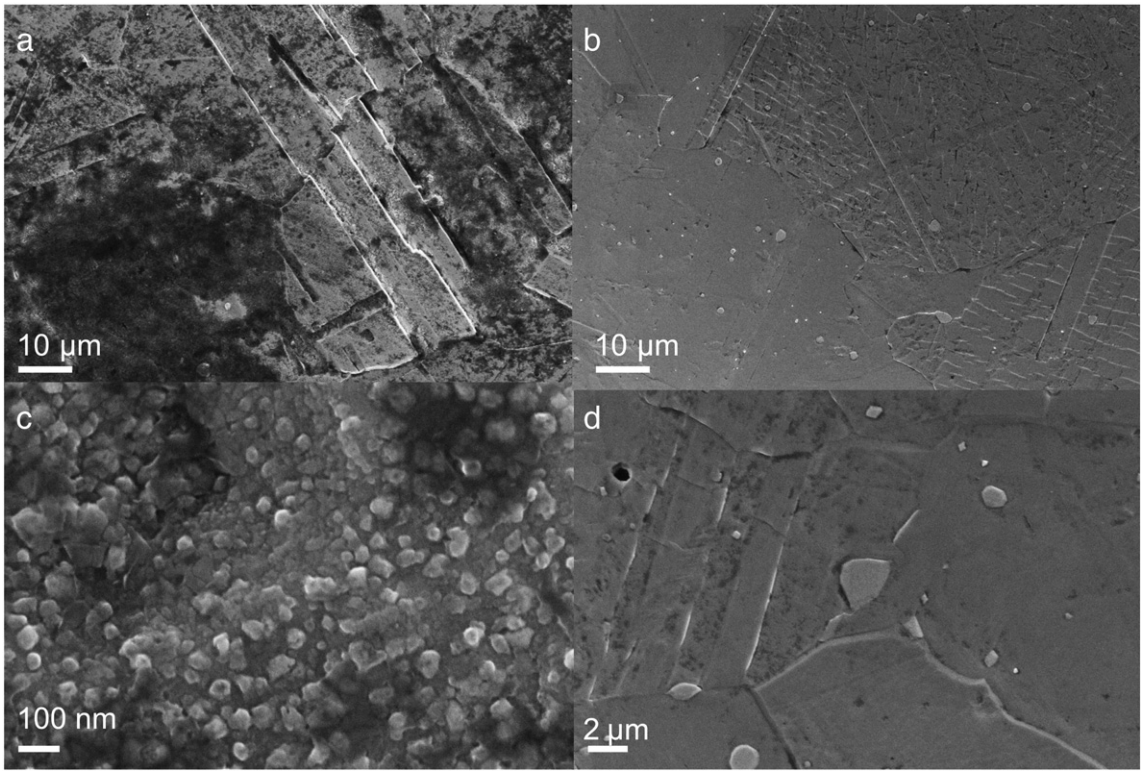

Fig. 12. Surface morphology as observed by SEM for PIII treated samples after 24 h corrosion testing: a and c) 550 °C; and b and d) 350 °C at different magnifications.

nitriding behaviour. At even higher processing temperatures, the formation of CrN precipitates result in a complete breakdown of the surface passivation as no more mobile chromium is available.

Nevertheless, caused by a much higher toxicity of cobalt containing nanoparticles reported in the literature, a beneficial surface treatment for temporary CoCr based implants is envisaged here as the wear resistance is improved to a similar content or even more than the corrosion resistance is compromised for processing temperatures of 350 °C or below. However, only Co ions are released while no release of toxic Cr(VI) or Ni(II) was observed, which were incorporated into the partial passivation layer. At the same time more than 50% of the original layer was removed during the presented corrosion experiments for the 550 °C implanted sample during the process, in contrast to slightly less than 20% for the sample processed at 350 °C. As a modified layer thickness of more than 5–10 μm is impractical due to the large increase in processing time at lower temperatures, a combined abrasive wear and corrosive attack will lead to a removal of this surface layer within less than 12 months, precluding permanent joint components from these applications. Cell culture tests are already in progress to quantify the exact interplay of corrosion and wear products.

Acknowledgments

The work presented in this paper was made possible in part by funding from the German Federal Ministry of Education and Research (BMBF, PtJ-Bio, 0313909). D. Hirsch is acknowledged for providing the SEM viewgraphs. Additionally, support from Innovation Department of Navarra Government within the BIOCOAT project is acknowledged.

References

[1] E. Wintermantel, S.-W. Ha, Medizintechnik mit biokompatiblen Werkstoffen und Verfahren, Springer, Berlin, 2002.
[2] M. Geetha, A.K. Singh, R. Asokamani, A.K. Gogia, Prog. Mater. Sci. 54 (2009) 397.
[3] S. Virtanen, I. Milošev, E. Gomez-Barrena, R. Trebše, J. Salo, Y.T. Konttinen, Acta Biomater. 4 (2008) 468.
[4] H. Ha, H.B. Kwak, S.W. Lee, H.M. Jin, H.M. Kim, H.H. Kim, H. Ha, Z.H. Lee, Exp. Cell Res. 301 (2004) 119.
[5] K.D. Merkel, J.M. Erdmann, K.P. McHugh, Y. Abu-Amer, F.P. Ross, S.L. Teitelbaum, Am. J. Pathol. 154 (1999) 203.
[6] J. Gallo, M. Raska, F. Mrazek, M. Petrek, Physiol. Res. 57 (2008) 339.
[7] A. Sabokbar, R. Pandey, J.M. Quinn, N.A. Athanasou, Arch. Orthop. Trauma. Surg. 117 (1998) 136.
[8] M.C. Pereira, M.L. Pereira, J.P. Sousa, Biomater. 20 (1999) 2193.
[9] C. Wolner, G.E. Nauer, J. Trummer, V. Putz, S. Tschegg, Mater. Sci. Eng. C 26 (2006) 34.
[10] D.G. Olmedo, D.R. Tasat, M.B. Guglielmotti, R.L. Cabrini, J. Mater. Sci. Mater. Med. 19 (2008) 3049.
[11] K.J. Kim, Y. Kobayashi, T. Itoh, Clin. Orthop. 352 (1998) 46.
[12] Y. Nakashima, D.H. Sun, M.C. Trindade, W.J. Maloney, S.B. Goodman, D.J. Schurman, R.L. Smith, J. Bone Joint Surg. Am. 81 (1999) 603.
[13] G. Oberdörster, E. Oberdörster, J. Oberdörster, Environ. Health Perspect. 113 (2005) 823.
[14] C.J. Kirkpatrick, W. Mohr, O. Haferkamp, Res. Exp. Med. 181 (1982) 259.
[15] S.A. Shabalovskaya, Int. Mater. Rev. 46 (2001) 233.
[16] K. Peters, H. Schmidt, R.E. Unger, G. Kamp, F. Pröls, B.J. Berger, C.J. Kirkpatrick, Mol. Cell. Biochem. 270 (2005) 157.
[17] S. Patntirapong, P. Habibovic, P.V. Hauschka, Biomater. 30 (2009) 548.
[18] D.F. Williams, in: D.F. Williams (Ed.), Biocompatibility of Clinical Materials, vol. I, CRC Press, Boca Raton, 1981, p. 99.
[19] T. Hanawa, S. Hiromoto, K. Asami, Appl. Surf. Sci. 183 (2001) 68.
[20] A.W.E. Hodgson, S. Kurz, S. Virtanen, V. Fervel, C.-O.A. Olsson, S. Mischler, Electrochim. Acta 49 (2004) 2167.
[21] M.A. Wimmer, J. Loos, M. Heitkemper, A. Fischer, Wear 250 (2001) 129.
[22] F.F. Hennig, H.J. Raithel, K.H. Schaller, J.R. Döhler, J. Trace Elem. Electrolytes Health Dis. 6 (1992) 239.
[23] T. Hanawa, Mater. Sci. Eng. C 24 (2004) 745.
[24] J. Chen, X.Y. Li, T. Bell, H. Dong, Wear 264 (2007) 157.
[25] O. Öztürk, U. Türkan, A.E. Eroğlu, Surf. Coat. Technol. 200 (2006) 5687.
[26] R. Wei, T. Booker, C. Rincon, J. Arps, Surf. Coat. Technol. 186 (2004) 305.
[27] B.R. Lanning, R. Wei, Surf. Coat. Technol. 186 (2004) 314.
[28] I.-M. Eichentopf, A. Lehmann, J. Lutz, J.W. Gerlach, S. Mändl, Plasma Processes Polym. 4 (2007) S44.
[29] J. Lutz, J.W. Gerlach, S. Mändl, Phys. Stat. Sol. 205 (2008) 980.
[30] J. Lutz, S. Mändl, Nucl. Instrum. Meth. B 267 (2009) 1522.
[31] J. Lutz, S. Mändl, Surf. Coat. Technol. 204 (2010) 3043.
[32] S. Mändl, D. Manova, H. Neumann, M.T. Pham, E. Richter, B. Rauschenbach, Surf. Coat. Technol. 200 (2005) 104.
[33] ASTM Standard F90-01: Standard Specification for Wrought Cobalt-20Chromium-15Tungsten-10Nickel Alloy for Surgical Implant Applications (UNS R30605), ASTM International, West Conshohocken, 2005.
[34] D. Manova, S. Mändl, B. Rauschenbach, Plasma Sources Sci. Technol. 10 (2001) 423.
[35] J. Lutz, Diffusion Behavior and Phase Formation for Ion Implanted Autenitic Metal Alloys, PhD thesis, Leipzig 2010.
[36] C. Diaz, J. Lutz, S. Mändl, J.A. García, R. Martínez, R.J. Rodríguez, Nucl. Instrum. Meth. B 267 (2009) 1630.
[37] T. Hryniewicz, R. Rokicki, K. Rokosz, Mater. Lett. 62 (2008) 3073.
[38] E. McCafferty, Corros. Sci. 44 (2002) 1393.
[39] H. Dong, Inter. Mat. Rev. 55 (2010) 65.
[40] S. Mändl, Plasma Processes Polym. 4 (2007) 239.
[41] T. Christiansen, M.A.J. Somers, Metall. Mater. Trans. A 37 (2006) 675.
[42] D. Manova, J. Lutz, S. Mändl, Surf. Coat. Technol. 204 (2010) 2875.
[43] B. Beverskog, I. Puigdomenech, Corros. Sci. 39 (1997) 969.
[44] J. Ponti, E. Sabbioni1, B. Munaro, F. Broggi, P. Marmorato, F. Franchini, R. Colognato, F. Rossi, Mutagenes 24 (2009) 439.
[45] R. Colognato, A. Bonelli, J. Ponti, M. Farina, E. Bergamaschi, E. Sabbioni, L. Migliore, Mutagenes. 23 (2008) 377.